

M2M-GAN: Many-to-Many Generative Adversarial Transfer Learning for Person Re-Identification

Wenqi Liang, Guangcong Wang, Jianhuang Lai, Junyong Zhu
School of Data and Computer Science, Sun Yat-sen University, China

Abstract

Cross-domain transfer learning (CDTL) is an extremely challenging task for the person re-identification (ReID). Given a source domain with annotations and a target domain without annotations, CDTL seeks an effective method to transfer the knowledge from the source domain to the target domain. However, such a simple two-domain transfer learning method is unavailable for the person ReID in that the source/target domain consists of several sub-domains, e.g., camera-based sub-domains. To address this intractable problem, we propose a novel Many-to-Many Generative Adversarial Transfer Learning method (M2M-GAN) that takes multiple source sub-domains and multiple target sub-domains into consideration and performs each sub-domain transferring mapping from the source domain to the target domain in a unified optimization process. The proposed method first translates the image styles of source sub-domains into that of target sub-domains, and then performs the supervised learning by using the transferred images and the corresponding annotations in source domain. As the gap is reduced, M2M-GAN achieves a promising result for the cross-domain person ReID. Experimental results on three benchmark datasets Market-1501, DukeMTMC-reID and MSMT17 show the effectiveness of our M2M-GAN.

Introduction

Person re-identification aims to retrieve person images across non-overlapping camera views given a probe image. Recently, a wide range of deep models, which uses classification loss (Deng et al. 2018; Zhuo et al. 2018), triplet-based loss (Wang et al. 2016; Ding et al. 2015; Wang, Lai, and Xie 2017) and verification loss (Li et al. 2014; Chen, Guo, and Lai 2015), achieve a significant improvement for the person ReID community. To further improve the performance, a lot of methods even exploit extra expensive annotations, e.g., keypoint annotations (Su et al. 2017; Zhao et al. 2017a), attribute annotations and semantic segmentation annotations (Kalayeh et al. 2018; Song et al. 2018). However, when applied to a new specific scenario, these methods require annotators to re-label a large amount of annotations to obtain a good performance. Motivated by this key point, an intuitive question arises: can we exploit

Copyright © 2019, Association for the Advancement of Artificial Intelligence (www.aaai.org). All rights reserved.

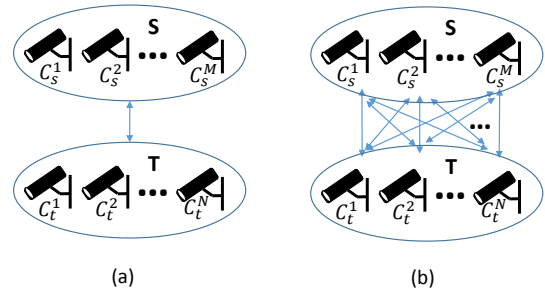


Figure 1: Classical one-to-one cross-domain transfer learning method vs. Our M2M-GAN method. A source domain S contains M camera-based sub-domains and a target domain T contains N ones. (a) Coarse one-to-one domain transferring method: it directly performs the transfer learning from a source domain to a target domain without considering camera-based sub-domains. (b) Our many-to-many transferring method (M2M-GAN): all pairs of sub-domain transferring relationships are optimized in a unified process by sharing parameters.

knowledge from an existing labeled dataset (labeled source domain) and then transfer it to a target scenario (unlabeled target dataset)?

A common approach for this question is to pre-train a model in a source domain and directly apply it to a target domain. However, there is a large gap between the source domain and the target domain in person ReID due to different lighting conditions, backgrounds, viewpoints, etc. Can we narrow the domain gap by exploiting the relationship between the source domain and the target domain? Recent cross-domain person ReID approaches address this issue by using a two-stage approach, i.e., transferring the labeled source domain to the target domain by using generative adversarial networks (GANs) and then performing supervised learning by using labeled transferred images. So, how to translate the labeled source domain to the target domain (the first stage) is the key point to the cross-domain transfer learning (CDTL) of person ReID.

Existing CDTL methods of person ReID (Deng et al. 2018; Wei et al. 2018) simply formulates CDTL as a classical one-to-one cycle generative adversarial model (Cycle-

GAN) (Zhu et al. 2017), which is employed for image style transferring between two domains, as shown in Figure 1 (a). However, one-to-one CDTL models neglect the fact that the source/target domain naturally consists of many sub-domains, i.e., camera-based sub-domains. In a source/target domain (dataset), feature representations across disjoint camera views of the same person follow different distributions due to the changes of viewpoints, lighting conditions and camera features (Chen, Zheng, and Lai 2015). The ignorance of different camera-based sub-domains confuses GANs (GANs do not know which sub-domain should be generated) and thus deteriorates the domain adaptation performance.

Inspired by this point, one would think distinguishing different camera-based sub-domains in the source/target domain may be beneficial for a CDTL ReID system. Given a CDTL ReID system that contains M source sub-domains and N target sub-domains, a natural approach to this problem is training $M \times N$ separate CycleGANs, respectively. As an initial attempt, Wei et al. (Wei et al. 2018) tried to transfer a large-scale dataset to a small-scale dataset with two cameras. To simplify, they do not distinguish different source sub-domains and only consider two target sub-domains by using two CycleGANs for CDTL. When applied to a large-scale dataset (e.g., MSMT17 with 15 cameras), they pointed out the expensive computational cost of separate CycleGANs for all pairs of source-to-target sub-domains and directly use classical one-to-one CDTL to reduce the model’s complexity on large-scale datasets.

Considering the drawbacks of these cross-domain ReID methods, we propose a novel many-to-many generative adversarial transfer learning method (M2M-GAN) that takes multiple source sub-domains and multiple target sub-domains into consideration and performs each sub-domain transferring mapping from the source domain to the target domain in a unified optimization process, as shown in Figure 1 (b). To accomplish this, the source sub-domain label l_s^i and the target sub-domain label l_t^j are embedded into an image x_{s_i} , which guides a generator to translate the image x_{s_i} from the source sub-domain S_i to the target sub-domain T_j and vice versa. With the guided information, M2M-GAN can easily address the many-to-many CDTL for person ReID.

Compared with $M \times N$ separate CycleGANs, our M2M-GAN method includes several fundamental properties. First, $M \times N$ pair-wise sub-domain transferring mappings (GANs) are naturally integrated into one M2M-GAN model with $1/(M \times N)$ parameters. For example, the Market-1501 dataset contains 6 cameras and the MSMT17 dataset contains 15 cameras, and thus there are 90 transferring mappings in all. M2M-GAN only needs $1/90$ of the parameters compared with $M \times N$ separate CycleGANs. Second, the training time of M2M-GAN is also significantly reduced due to the joint optimization. Third, M2M-GAN provides a good solution for many-to-many CDTL in person ReID. M2M-GAN jointly optimizes $M \times N$ transferring mappings that share the similar transferring knowledge while separate CycleGANs neglect this key point and have limited data (e.g., the dataset is split into $M \times N$ pairs of source-to-target subsets) for the learning of each transferring mapping, which

may encounter the over-fitting problem.

Overall, this paper makes three main contributions:

- First, as far as we know, it is the first attempt to address the many-to-many cross-domain transfer learning (CDTL) problem for person ReID. We highlight that many-to-many CDTL is much more appropriate for cross-domain person ReID than one-to-one CDTL because feature representations across disjoint camera views of the same person follow different distributions.
- Second, to solve the many-to-many CDTL problem for person ReID, we propose a novel many-to-many generative adversarial transfer learning (M2M-GAN), which translates the image style from source sub-domains to target sub-domains with less training time, fewer parameters and a better performance. Moreover, we also integrate a mask-based identity preserve loss, a camera-based sub-domain classification loss into the proposed framework.
- Third, extensive experiments show that the proposed method is effective in three benchmark datasets, i.e., Market-1501, DukeMTMC-reID and MSMT17.

Related Work

Recent deep models have shown remarkable success in person ReID by using different types of loss, e.g., classification loss, verification loss and triplet loss. For example, generalized similarity measure methods (Wang et al. 2016; Lin et al. 2016) are naturally integrated into deep networks. Feng et al. (Feng, Lai, and Xie 2018) proposed a view-specific person ReID framework by leveraging the classification loss, center loss and Euclidean distance constraint. Ding et al. (Ding et al. 2015) proposed an image-based triplet loss to reduce the computational cost. Based on the image-based triplet loss, Wang et al. (Wang, Lai, and Xie 2017) extended a kNN-triplet for the image-to-video person ReID.

Recently, a rich variety of person ReID methods pay attention to extra information to further improve the performance. For example, Li et al. (Li et al. 2017) used the global body-based feature, latent person parts and local part-based features for person representation. Zhao et al. (Zhao et al. 2017b) proposed to decompose the human body into regions (parts) for person matching and aggregate the similarities computed between the corresponding regions as the overall matching score. Su et al. (Su et al. 2017) introduced a pose-driven deep convolution model to alleviate the pose variations and learn robust feature representations from both the global images and different local parts. Zhao et al. (Zhao et al. 2017a) introduced a SpindleNet based on human body region guided multi-stage feature decomposition and tree-structured competitive feature fusion. Song et al. (Song et al. 2018) introduced the binary segmentation masks to construct synthetic RGB-Mask pairs as inputs, and designed a mask-guided contrastive attention model to learn features separately from the body and background regions. Kalayeh (Kalayeh et al. 2018) et al. attempted to integrate human semantic parsing into person ReID and achieved a competitive result. Wang et al. (Wang et al. 2019) proposed a st-ReID

method with a spatial-temporal constraint, which dramatically outperformed current state-of-the-arts.

Instead of focusing on supervised person ReID, some studies attempt to transfer the knowledge from a labeled domain to an unlabeled domain, which arises in many real-world person ReID applications. Cross-domain transfer learning (CDTL) methods in person ReID can be categorized into two groups, i.e., single-stage transferring and two-stage transferring. Single-stage CDTL methods directly build a relationship between a source domain and a target domain at the feature level. For example, Ganin et al. (Ganin et al. 2016) performed the domain adaption by adding a domain classifier and a gradient reversal layer. Differently, two-stage CDTL methods first generate new training images by translating the data distribution of the source domain to that of the target domain at the image level. Then the transferred images with source domain annotations are used for supervised learning. For example, Deng et al. (Deng et al. 2018) proposed to preserve self-similarity of an image before and after translation and domain-dissimilarity of a translated source image and a target image. However, this method simply regards the person ReID transfer learning problem as a one-to-one domain adaption problem but neglects the fact that a source/target domain contains several sub-domains. Wei et al. (Wei et al. 2018) proposed a person transfer method to bridge domain gap in a one-to-one manner and also implicitly used two separate CycleGANs for a small-scale dataset transferring, which can be regarded as a one-to-two CDTL. However, they did not distinguish different source sub-domains and pointed out that training many separate CycleGANs is quite expensive and unavailable for large-scale datasets that contains lots of cameras. Our approach differs from these methods, as the proposed model explicitly formulate the cross-domain person ReID problem as a many-to-many adversarial transfer learning problem.

Concurrently, other unsupervised domain adaptation methods (Zhong et al. 2018b; Zhong et al. 2018a), simply using CycleGAN (Zhu et al. 2017) or StarGAN (Choi et al. 2018), are also developed. These methods focus on the image style translation between target sub-domains while the images in the source domain are ignored or simply used to form negative pairs for model training. This pipeline pays attention to the intra-domain generative adversarial transfer learning while our M2M-GAN method aims for the inter-domain generative adversarial transfer learning.

Proposed Method

Problem Definition.

Cross-domain transfer learning (CDTL) of the person ReID is featured in two aspects. First, it contains a labeled source domain and an unlabeled target domain. The goal of CDTL in person ReID is to transfer the distribution of the source domain to that of the target domain conceptually. Second, the source/target domain contains several sub-domains, i.e., camera-based sub-domains. Different camera-based sub-domains in the same domain have something in common but differ a lot from each other due to different lighting conditions, backgrounds, and viewpoints.

Formally, let S denote a labeled source domain and T denote an unlabeled target domain. S contains M sub-domains, denoting $S_1, S_2, \dots, S_i, \dots, S_M$. The corresponding cameras are $C_s^1, C_s^2, \dots, C_s^i, \dots, C_s^M$. T contains N sub-domains, denoting $T_1, T_2, \dots, T_j, T_N$. The corresponding cameras are $C_t^1, C_t^2, \dots, C_t^j, \dots, C_t^N$. The goal of many-to-many CDTL in person ReID is to translate the image style from S_i to T_j given any i and j , where $1 \leq i \leq M$ and $1 \leq j \leq N$. Let a labeled image $(x_{s_i}, y_{s_i}) \in S_i$. The subscript of x denotes which sub-domain the image follows. Many-to-many CDTL translates the real image x_{s_i} to the fake image $x_{t_j}^*$ such that $x_{t_j}^*$ follows the distribution of T_j . The fake image $x_{t_j}^*$ and the corresponding label y_{s_i} are used to supervised learning for person ReID.

Formulation of M2M-GAN.

Supervised person ReID methods (Chen, Zheng, and Lai 2015; Feng, Lai, and Xie 2018) have revealed that feature representations across disjoint camera views of the same person follow different distributions due to the changes of viewpoints, lighting conditions and camera features. Directly using CycleGAN to transfer the image styles between S and T will confuse the generators because S and T contain different sub-domains and generators do not know which source sub-domain or target sub-domain should be generated. Without considering the existing of sub-domains, CycleGAN can hardly offer an optimal solution for the many-to-many CDTL problem.

To solve this problem, a M2M-GAN is proposed in this paper. The main idea behind our M2M-GAN is to embed the source sub-domain label information l_{s_i} and the target sub-domain label information l_{t_j} into the image x_{s_i} and guide the generators to generate the desired image $x_{t_j}^*$. By doing this, generators know which target sub-domain it will generate and which source sub-domain it comes from during the source-to-target training process (note that the target-to-source training process is the same). With the guided feature maps, M2M-GAN can jointly optimize $M \times N$ transferring mappings from the source sub-domains to the target sub-domains in a unified process. For simplicity, we only consider the source-to-target translation. We embed this guided information into an image by

$$x_{embed}^{s_i t_j} = [x_{rgb}, B_s^i, B_t^j] \quad (1)$$

where $[\cdot, \cdot]$ represents channel concatenation, x_{rgb} represents a RGB image of size $(3, h, w)$, B_s^i represents a binary tensor of size (M, h, w) , B_t^j represents a binary tensor of size (N, h, w) , and $x_{embed}^{s_i t_j}$ denotes a tensor of size $(M + N + 3, h, w)$. The i -th channel of B_s^i is “one” value, denoting that x_{rgb} comes from the i -th source sub-domain and the remaining $M - 1$ channels are “zero” values. The j -th channel of B_t^j is “one” value, denoting that x_{rgb} will be translated to the j -th target sub-domain and the remaining $N - 1$ channels are “zero” values. In this way, $x_{embed}^{s_i t_j}$ guides M2M-GAN to translate x_{rgb} into a 3-channel fake image x_{rgb}^* from S_i to T_j . In the similar way, we obtain $x_{embed}^{t_j s_i}$.

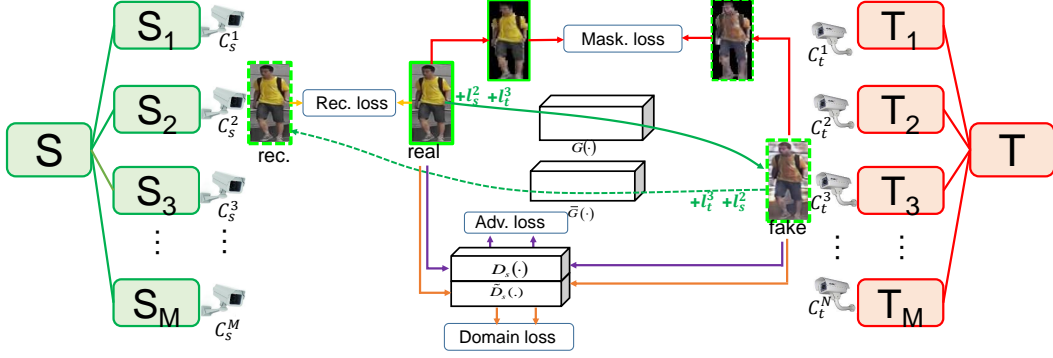


Figure 2: The proposed M2M-GAN architecture. For simplicity, it only describes a pair of sub-domain transferring from a source sub-domain S_i to a target sub-domain T_j . Given a source image x_{s_i} with a source sub-domain label l_{s_i} and a target sub-domain label l_{t_j} that is the desired transferred image style, we use cycle loss, adversarial loss, identity loss and reconstruction loss to train M2M-GAN and obtain a good transferred (fake) image $x_{t_j}^*$ in the target sub-domain. The same process are performed during the target-to-source image style transferring. (Best viewed in color)

Overall, we use two generators, two discriminators and two domain classifiers, among which half of them are used for the source-to-target transferring while the rest of them are used for the target-to-source transferring. We use a cycle loss, an adversarial loss, an identity loss and a reconstruction loss to constrain the networks to obtain a good transferred (fake) image $x_{t_j}^*$ for supervised learning. Figure 2 shows the overview of our M2M-GAN for the many-to-many cross-domain person ReID. Details.

Adversarial Loss. To translate the distribution of the source sub-domain S_i to that of the target sub-domain T_j , the adversarial loss is used

$$L_{adv}(G, D_t) = \sum_{i=1}^M \sum_{j=1}^N (\mathbb{E}_{x_{t_j}} [\log D_t(x_{t_j})] + \mathbb{E}_{x_{s_i}} [\log(1 - D_t(G(x_{s_i}, l_s^i, l_t^j)))])) \quad (2)$$

where G attempts to generate a fake image $G(x_{s_i}, l_s^i, l_t^j)$ that is indistinguishable from the images in T_j given an image x_{s_i} and domain labels l_s^i and l_t^j while D_t attempts to distinguish between real and fake images in T_j . Mathematically, G attempts to minimize $L_{adv}(G, D_t)$ while D_t attempts to maximize $L_{adv}(G, D_t)$.

In the same way, we obtain a similar adversarial loss for the transferring mapping from the target sub-domain T_j to the source sub-domain S_i , i.e., $L_{adv}(\bar{G}, D_s)$, where \bar{G} denotes a generator which is used for the target-to-source transferring and D_s is used to distinguish between real and fake images in S_i .

Reconstruction Loss. Reconstruction loss, also implicitly termed cycle loss, is widely used in unsupervised auto-encoder. It aims to regularize the mappings such that $x_{s_i} \rightarrow G(x_{s_i}, l_s^i, l_t^j) \rightarrow \bar{G}(G(x_{s_i}, l_s^i, l_t^j), l_t^j, l_s^i) \approx x_{s_i}$ and $x_{t_j} \rightarrow \bar{G}(x_{t_j}, l_t^j, l_s^i) \rightarrow G(\bar{G}(x_{t_j}, l_t^j, l_s^i), l_s^i, l_t^j) \approx x_{t_j}$. Considering

these two constraints, we compute the reconstruction loss by

$$L_{rec}(G, \bar{G}) = \sum_{i=1}^M \sum_{j=1}^N (||x_{s_i} - \bar{G}(G(x_{s_i}, l_s^i, l_t^j), l_t^j, l_s^i)||_1 + ||x_{t_j} - G(\bar{G}(x_{t_j}, l_t^j, l_s^i), l_s^i, l_t^j)||_1) \quad (3)$$

Mask-based Identity Preserve Loss. To further preserve the content of the person images, we use Mask-RCNN to perform person segmentation and attempt to preserve the foreground of the images before and after generating fake images. Without the identity preserve loss, it is hard for M2M-GAN to preserve the content of person images due to large cross-domain variations, e.g., different person identities, significant changes in illumination, background clutter, pose, viewpoint, and occlusion. We compute the mask-based identity preserve loss by

$$L_{mask}(G, \bar{G}) = \sum_{i=1}^M \sum_{j=1}^N (||x_{s_i} \bullet M(x_{s_i}) - G(x_{s_i}, l_s^i, l_t^j) \bullet M(x_{s_i})||_2 + ||x_{t_j} \bullet M(x_{t_j}) - \bar{G}(x_{t_j}, l_t^j, l_s^i) \bullet M(x_{t_j})||_2) \quad (4)$$

where $M(\cdot)$ takes an image as input and output a person mask. \bullet denotes a pixel-wise multiplication operator.

Sub-domain Classification Loss. To distinguish the sub-domain labels of a real/fake image, we use the cross entropy loss. The losses of real and fake images are computed by

$$L_{dom}^r(\tilde{D}_s, \tilde{D}_t) = \sum_{i=1}^M \sum_{j=1}^N ((L_{ce}(\tilde{D}_s(x_{s_i}), l_s^i)) + L_{ce}(\tilde{D}_t(x_{t_j}), l_t^j)) \\ L_{dom}^f(G, \bar{G}, \tilde{D}_s, \tilde{D}_t) = \sum_{i=1}^M \sum_{j=1}^N ((L_{ce}(\tilde{D}_s(G(x_{s_i}, l_s^i, l_t^j)), l_t^j)) + L_{ce}(\tilde{D}_t(\bar{G}(x_{t_j}, l_t^j, l_s^i), l_s^i))) \quad (5)$$

where the sub-domain classifiers \tilde{D}_s and \tilde{D}_t share the parameters with D_s and D_t , respectively. $L_{ce}(\cdot, \cdot)$ denotes the cross entropy loss.

Full objective. Considering all the loss described above, we decompose this two-player minimax optimization problem into two parts

$$\begin{aligned}
 L_D &= -L_{adv}(G, D_t) - L_{adv}(\bar{G}, D_s) + \lambda_1 L_{dom}^r(\tilde{D}_s, \tilde{D}_t) \\
 L_G &= L_{adv}(G, D_t) + L_{adv}(\bar{G}, D_s) \\
 &\quad + \lambda_1 L_{dom}^f(G, \bar{G}, \tilde{D}_s, \tilde{D}_t) \\
 &\quad + \lambda_2 L_{mask}(G, \bar{G}) + \lambda_3 L_{rec}(G, \bar{G})
 \end{aligned}
 \tag{6}$$

where λ_1 , λ_2 and λ_3 control the relative importance of the four objectives. We alternately optimize L_D and L_G . When optimizing L_D , we fix G, \bar{G} to optimize $D_s, D_t, \tilde{D}_s, \tilde{D}_t$, and vice versa.

Feature Learning.

After the transferring from source sub-domains to target sub-domains, we obtain lots of transferred fake images that follow the distributions of target sub-domains. With these transferred fake images and their corresponding raw identity labels, we can perform feature learning by using supervised person ReID methods. Note that we do not use any label in target domain. In this paper, we do not focus on how to learn a robust feature representation. Therefore, we simply use a conventional classification network (ResNet-50) as a base model.

Implementation.

Network Architecture.

Following (Zhu et al. 2017), M2M-GAN has two generators and two discriminators (discriminators and classifiers share parameters). The generative networks consist of two stride-2 convolution layers, six residual blocks and two stride-1/2 fractionally-strided convolution layers. We also use instance normalization (Ulyanov, Vedaldi, and Lempitsky 2016) for generators. For discriminators, we use PatchGANs (Isola et al. 2017).

As for feature learning networks, we use a base ResNet-50, followed by a 512-dim FC layer, a Batch Normalization layer, a ReLU layer, a dropout layer, a n -dim FC layer (n denotes the number of person identities) and a Cross Entropy layer. During testing, we extract the features from the Average Pooling layer.

Training.

When training the M2M-GAN networks, we use Adam with $\beta_1 = 0.5$ and $\beta_2 = 0.999$. Following StarGAN (Choi et al. 2018), we perform one step of optimizing generators after five steps of optimizing discriminators. We train M2M-GAN with a learning rate of 0.0001 for the first 100,000 iterations and linearly decay the learning rate to 0 over the next 100,000 iterations. The batch size is set to 16. After training M2M-GAN, we generate N fake images that follow N target sub-domains respectively for each source image. The fake images are further used for feature learning. We set $\lambda_1 = 1$, $\lambda_2 = 100$, and $\lambda_3 = 10$.

When training the feature learning networks, the pre-trained ResNet-50 model is used and further fine-tuned on the translated target domain. We use SGD with mini-batch

size of 256. The learning rate is initialized to 0.1 for FC layers and 0.01 for other layers. After 30 epochs, the learning rate is divided by 10. We resize images to 256×128 . We train these networks for 40 epochs. Note that only the training set of the source domain and unlabeled training set of the target domain are used for both M2M-GAN training and feature learning.

Experiments

In this section, we evaluate our M2M-GAN method on three large-scale person ReID benchmark datasets, i.e., Market-1501, DukeMTMC-reID and MSMT17, and present ablation studies to reveal the importance of each main component/factor of our method. We then reveal the benefits of the M2M-GAN model compared with state-of-the-art methods. We use CMC and mAP for evaluation.

Datasets. The Market-1501 dataset with six cameras is collected in Tsinghua University. Overlap exists among different cameras. Overall, this dataset contains 32,668 annotated bounding boxes of 1,501 identities. Among them, 12,936 images from 751 identities are used for training, and 19,732 images from 750 identities plus distractors are used for gallery. As for query, 3,368 hand-drawn bounding boxes from 750 identities are adopted. Each annotated identity is present in at least two cameras.

DukeMTMC-reID has 8 cameras. There are 1,404 identities appearing in more than two cameras and 408 identities (distractor ID) who appear in only one camera. Specially, 702 IDs are selected as the training set and the remaining 702 IDs are used as the testing set. In the testing set, one query image is picked for each ID in each camera and the remaining images are put in the gallery. In this way, there are 16,522 training images of 702 identities, 2,228 query images of the other 702 identities and 17,661 gallery images (702 ID + 408 distractor ID).

MSMT17 is the largest person re-identification dataset. It contains 15 cameras, i.e., 12 outdoor cameras and 3 indoor cameras. Four days with different weather conditions in a month are selected for video collection. For each day, 3 hours of videos taken in the morning, noon, and afternoon, respectively, are selected for pedestrian detection and annotation. The final raw video set contains 180 hours of videos, 12 outdoor cameras, 3 indoor cameras, and 12 time slots. Faster RCNN is utilized for pedestrian bounding box detection. Finally, 126,441 bounding boxes of 4,101 identities are annotated.

Evaluation and Model Analysis

To evaluate the effectiveness of M2M-GAN, we conduct different kinds of ablation studies according to the CDTL setting.

Effectiveness of M2M-GAN. To evaluate the effectiveness of M2M-GAN, one of three datasets is used as the target domain and the other two are used as source domains, respectively. Therefore, there are six transferring combinations. We design several experimental comparisons to validate the points discussed in our paper. Note that we use the same feature learning networks and the same training scheme in all experiments.

| Methods | D->MA | | MA->D | | D->MS | | MS->D | | MA->MS | | MS->MA | |
|---------------------|-------|------|-------|------|-------|------|-------|------|--------|------|--------|------|
| | R1 | mAP | R1 | mAP | R1 | mAP | R1 | mAP | R1 | mAP | R1 | mAP |
| supervised | 85.4 | 66.9 | 76.5 | 57.1 | 61.3 | 30.8 | 76.5 | 57.1 | 61.3 | 30.8 | 85.4 | 66.9 |
| Pre-training | 50.4 | 23.6 | 38.1 | 21.4 | 20.2 | 6.7 | 53.5 | 32.5 | 14.2 | 4.5 | 51.5 | 25.5 |
| one-to-one | 47.4 | 21.5 | 43.1 | 24.1 | 24.7 | 7.8 | 51.1 | 30.0 | 22.7 | 7.6 | 46.1 | 21.1 |
| many-to-many (Ours) | 57.5 | 26.8 | 49.6 | 26.1 | 35.3 | 11.2 | 56.6 | 33.3 | 30.9 | 10.1 | 53.4 | 25.2 |

Table 1: Effectiveness of M2M-GAN. There are six transferring combinations between three datasets. ‘‘D’’, ‘‘MA’’ and ‘‘MS’’ denotes DukeMTMC-reID, Market-1501 and MSMT17, respectively.

We first validate the point that although cross-domain transfer learning is important in person ReID, it undergoes a serious degradation compared with supervised person ReID. We conduct two experiments according to these two methods, i.e., supervised person ReID (denoted as ‘‘Supervised’’) and directly transferring (denoted as ‘‘Directly transfer’’). ‘‘Supervised’’ is trained and tested on a labeled target domain. ‘‘Directly transfer’’ is trained on a labeled source domain and tested on a target domain. As shown in Table 1, we can see that the rank-1 accuracy of ‘‘Directly transfer’’ is dropped by $\sim 30\%$ compared with ‘‘Supervised’’, e.g., 35%, 38.4%, 41.1%, 23.0%, 47.1%, and 33.9% for six transferring processes, respectively. The reason is that there is a large distribution gap between two datasets collected in different scenarios.

We then validate the point that one-to-one CDTL method (denoted as ‘‘One-to-one’’) is inappropriate for the CDTL of person ReID. Compared with ‘‘Directly transfer’’, ‘‘One-to-one’’ obtains rank-1 accuracy of -3.0%, +5.0%, 4.5%, -2.4%, 8.5%, and -5.4% improvement for six transferring processes, respectively. For three transferring processes, ‘‘One-to-one’’ is better than ‘‘Directly transfer’’ while for the other three transferring processes, ‘‘Directly transfer’’ is even better than ‘‘One-to-one’’. The reason may be attributed to the fact that the ignorance of sub-domains of the source/target domain confuses GANs, i.e., GANs do not know which sub-domain should be generated.

Most importantly, We further validate the point that our many-to-many CDTL method (denoted as ‘‘Many-to-many’’) is better than both ‘‘Directly transfer’’ and ‘‘One-to-one’’ methods. Compared with ‘‘Directly transfer’’, our ‘‘Many-to-many’’ obtains rank-1 accuracy of 7.1%, 11.5%, 15.1%, 3.1%, 16.7%, and 1.9% for six transferring processes, respectively. These show that our ‘‘Many-to-many’’ can reduce the domain gap between a source domain and a target domain and thus improve the performance of cross-domain person ReID. Compared with ‘‘One-to-one’’, our ‘‘Many-to-many’’ obtains 10.1%, 6.5%, 10.6%, 5.5%, 8.2%, and 7.3% for six transferring processes, respectively. These show that it is necessary to take camera-based sub-domains into consideration because different camera-based sub-domains in the same domain follow different distributions. When considering the source/target sub-domain labels into CDTL, GANs know which source sub-domain the image comes from and which target sub-domain the image will be translated and thus improve the performance of cross-domain person ReID.

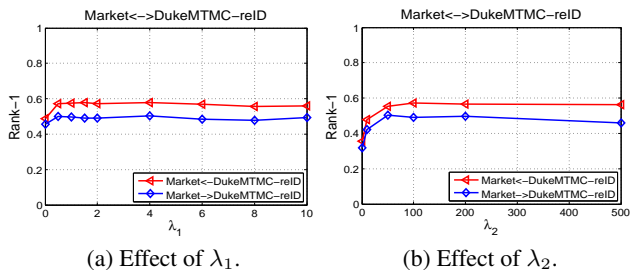


Figure 3: Influence of parameters.

Influence of parameters. To investigate the impact of two important parameters in our M2M-GAN, i.e., λ_1 and λ_2 , we conduct two sensitivity analysis experiments. As shown in Figure 3 (a) and (b), when λ_1 is in the range of 0.5~10.0 or λ_2 is in the range of 50~500, our model nearly keeps the best performance.

Effect of different feature learning schemes. To investigate the effect of different feature learning schemes, we conduct two experiments for evaluation. First, we use only fake target images and their corresponding source labels for training. Second, we use both fake target images and real source images with labels for training. The experimental results are shown in Table 3. It is observed that although real source images do not follow the distribution of the target domain, it is still beneficial to the overall performance. The reason is that it is difficult to transfer all the information from a source domain to a target domain. Therefore, it is reasonable to re-use source images to compensate for the loss of information during transferring.

Comparisons of computational cost. To analyze the computational cost of our M2M-GAN, we compare our M2M-GAN (denoted as ‘‘M2M.’’) with a brute-force many-to-many method that contains $M \times N$ separate CycleGANs (denoted as ‘‘Sper.’’), which is implicitly used in the recent work (Wei et al. 2018). As shown in Table 4, we can see that the model size of our ‘‘M2M.’’ nearly keeps the same with camera number increasing (the channels of first convolution kernel are affected) while the model size of ‘‘Sper.’’ is proportional to the camera number. When the camera number is large, ‘‘Sper.’’ is unavailable.

As for the training time, it is widely known that it costs much time to train a generative adversarial network because of an adversarial loss, e.g., half of a day. When training $M \times N$ separate CycleGANs on $M \times N$ pairs of source-

| Methods | D->MA | | MA->D | | D->MS | | MS->D | | MA->MS | | MS->MA | |
|---------------------------|-------------|-------------|-------------|-------------|-------------|-------------|-------------|-------------|-------------|-------------|-------------|-------------|
| | R1 | mAP | R1 | mAP | R1 | mAP | R1 | mAP | R1 | mAP | R1 | mAP |
| LOMO | 27.2 | 8.0 | 12.3 | 4.8 | - | - | 12.3 | 4.8 | - | - | 27.2 | 8.0 |
| Bow | 35.8 | 14.8 | 17.1 | 8.3 | - | - | 17.1 | 8.3 | - | - | 35.8 | 14.8 |
| EOLMA | 40.9 | - | - | - | - | - | - | - | - | - | - | - |
| UMDL | 34.5 | 12.4 | 18.5 | 7.3 | - | - | - | - | - | - | - | - |
| PUL | 45.5 | 20.5 | 30.0 | 16.4 | - | - | - | - | - | - | - | - |
| CAMEL | 54.5 | 26.3 | - | - | - | - | - | - | - | - | - | - |
| MMFA | - | - | 45.3 | 24.7 | - | - | - | - | - | - | - | - |
| PTGAN | 38.6 | - | 27.4 | - | 11.8 | 3.3 | - | - | 10.2 | 2.9 | - | - |
| SPGAN | 51.5 | 22.8 | 41.1 | 22.3 | - | - | - | - | - | - | - | - |
| SPGAN+LMP | 57.7 | 26.7 | 46.4 | 26.2 | - | - | - | - | - | - | - | - |
| TJ-AIDL | 58.2 | 26.5 | 44.3 | 23.0 | - | - | - | - | - | - | - | - |
| M2M-GAN (Ours) | 59.1 | 29.6 | 52.0 | 29.8 | 36.8 | 11.9 | 61.1 | 37.5 | 31.9 | 10.8 | 57.9 | 28.8 |
| M2M-GAN+LMP (Ours) | 63.1 | 30.9 | 54.4 | 31.6 | 35.5 | 10.5 | 61.7 | 37.2 | 32.2 | 9.7 | 60.8 | 29.7 |

Table 2: Comparisons to the State-of-the-Art. There are six transferring combinations between three datasets. ‘‘D’’, ‘‘MA’’ and ‘‘MS’’ denotes DukeMTMC-reID, Market-1501 and MSMT17, respectively. The compared methods are categorized into three groups. Group 1: handcrafted feature methods. Group 2: unsupervised person ReID methods. Group 3: cross-domain transfer learning methods.

| Methods | D->MA | | MA->D | |
|-----------|-------------|-------------|-------------|-------------|
| | R1 | mAP | R1 | mAP |
| fake | 57.5 | 26.8 | 49.6 | 26.1 |
| fake+real | 59.1 | 29.6 | 52.0 | 29.8 |

Table 3: Effect of different feature learning schemes.

| Meth. | D<->MA | MA<->MS | MS<->D |
|-------|----------------|----------------|----------------|
| Sper. | 52.60M*8*6 | 52.60M*6*15 | 52.60M*15*8 |
| M2M. | 106.47M | 106.58M | 106.60M |

Table 4: Comparisons of computational cost.

to-target sub-domains, we estimate that our ‘‘M2M.’’ is much faster than ‘‘Sper.’’ empirically, even though each CycleGAN is trained on smaller sub-domains.

Comparisons to the State-of-the-Art

In this section, we compare our M2M-GAN with state-of-the-art methods by selecting one dataset as the target domain and the other two as the source domains, respectively. Therefore, we obtain six pairs of transferring combinations. The results are shown in Table 2.

We compare our approach with eleven state-of-the-art methods, which can be grouped into three categories. The first group includes three representative unsupervised person ReID methods using handcrafted features, i.e., LOMO (Liao et al. 2015), Bow (Zheng et al. 2015) and EOLMA (Zhou et al. 2017). The experimental results clearly demonstrate the effectiveness of our M2M-GAN against the conventional handcrafted features, e.g., leading to 35.4% and 42.1% improvement on Market-1501 and DukeMTMC-reID respectively, compared with LOMO. The reason can be contributed to the fact that handcrafted features are inferior to

the deep features.

The second group includes three unsupervised person ReID methods, i.e., UMDL (Peng et al. 2016), PUL (Fan, Zheng, and Yang 2017), CAMEL (Yu, Wu, and Zheng 2017). Compared with handcrafted features, the performance of these methods are improved to some extent. However, these methods do not consider the relationship between a labeled dataset and an unlabeled dataset and are therefore inferior to cross-domain methods.

The third group includes five representative CDTL methods, i.e., PTGAN (Wei et al. 2018), SPGAN (Deng et al. 2018), CAMEL (Yu, Wu, and Zheng 2017), SPGAN+LMP (Deng et al. 2018), and TJ-AIDL (Wang et al. 2018). It is observed that our M2M-GAN outperforms all the competing methods. The main reason can be contributed the fact that our M2M-GAN takes camera-based source/target sub-domains into consideration and optimized in a unified process.

Conclusion

In this paper, we propose a novel Many-to-Many Generative Adversarial Transfer Learning method (M2M-GAN) takes multiple source sub-domains and multiple target sub-domains into consideration and performs each pair-wise sub-domain transferring from the source domain to the target domain in a unified optimization process. As a result, our M2M-GAN solve the many-to-many CDTL with less training time, fewer parameters and a better performance. Experimental results on three large-scale benchmark datasets show the effectiveness of our M2M-GAN. We intend to extend this work in two directions. First, we intend to generalize the M2M-GAN to a generalized CDTL problem with any kind of adversarial topology. Second, the sub-domains of M2M-GAN are not limited to the camera-based sub-domains and therefore M2M-GAN can be easily generalized to any many-to-many CDTL problem.

References

- [Chen, Guo, and Lai 2015] Chen, S.-Z.; Guo, C.-C.; and Lai, J.-H. 2015. Deep ranking for person re-identification via joint representation learning. *arXiv:1505.06821*.
- [Chen, Zheng, and Lai 2015] Chen, Y.-C.; Zheng, W.-S.; and Lai, J.-H. 2015. Mirror representation for modeling view-specific transform in person re-identification. In *IJCAI*.
- [Choi et al. 2018] Choi, Y.; Choi, M.; Kim, M.; Ha, J.-W.; Kim, S.; and Choo, J. 2018. Stargan: Unified generative adversarial networks for multi-domain image-to-image translation. In *CVPR*.
- [Deng et al. 2018] Deng, W.; Zheng, L.; Ye, Q.; Kang, G.; Yang, Y.; and Jiao, J. 2018. Image-image domain adaptation with preserved self-similarity and domain-dissimilarity for person re-identification. In *CVPR*.
- [Ding et al. 2015] Ding, S.; Lin, L.; Wang, G.; and Chao, H. 2015. Deep feature learning with relative distance comparison for person re-identification. *Pattern Recognition* 48(10):2993–3003.
- [Fan, Zheng, and Yang 2017] Fan, H.; Zheng, L.; and Yang, Y. 2017. Unsupervised person re-identification: Clustering and fine-tuning. *CoRR* abs/1705.10444.
- [Feng, Lai, and Xie 2018] Feng, Z.; Lai, J.; and Xie, X. 2018. Learning view-specific deep networks for person re-identification. *IEEE TIP* 27(7):3472–3483.
- [Ganin et al. 2016] Ganin, Y.; Ustinova, E.; Ajakan, H.; Germain, P.; Larochelle, H.; Laviolette, F.; Marchand, M.; and Lempitsky, V. S. 2016. Domain-adversarial training of neural networks. *Journal of Machine Learning Research* 17:59:1–59:35.
- [Isola et al. 2017] Isola, P.; Zhu, J.-Y.; Zhou, T.; and Efros, A. A. 2017. Image-to-image translation with conditional adversarial networks. In *CVPR*.
- [Kalayeh et al. 2018] Kalayeh, M. M.; Basaran, E.; Gökmen, M.; Kamasak, M. E.; and Shah, M. 2018. Human semantic parsing for person re-identification. In *CVPR*, 1062–1071.
- [Li et al. 2014] Li, W.; Zhao, R.; Xiao, T.; and Wang, X. 2014. Deepreid: Deep filter pairing neural network for person re-identification. In *CVPR*, 152–159.
- [Li et al. 2017] Li, D.; Chen, X.; Zhang, Z.; and Huang, K. 2017. Learning deep context-aware features over body and latent parts for person re-identification. In *CVPR*, 384–393.
- [Liao et al. 2015] Liao, S.; Hu, Y.; Zhu, X.; and Li, S. Z. 2015. Person re-identification by local maximal occurrence representation and metric learning. In *CVPR*, 2197–2206.
- [Lin et al. 2016] Lin, L.; Wang, G.; Zuo, W.; Xiangchu, F.; and Zhang, L. 2016. Cross-domain visual matching via generalized similarity measure and feature learning. *IEEE TPAMI* PP(99):1–1.
- [Peng et al. 2016] Peng, P.; Xiang, T.; Wang, Y.; Pontil, M.; Gong, S.; Huang, T.; and Tian, Y. 2016. Unsupervised cross-dataset transfer learning for person re-identification. In *CVPR*.
- [Song et al. 2018] Song, C.; Huang, Y.; Ouyang, W.; and Wang, L. 2018. Mask-guided contrastive attention model for person re-identification. In *The IEEE Conference on Computer Vision and Pattern Recognition (CVPR)*, 1179–1188.
- [Su et al. 2017] Su, C.; Li, J.; Zhang, S.; Xing, J.; Gao, W.; and Tian, Q. 2017. Pose-driven deep convolutional model for person re-identification. In *ICCV*, 3960–3969.
- [Ulyanov, Vedaldi, and Lempitsky 2016] Ulyanov, D.; Vedaldi, A.; and Lempitsky, V. S. 2016. Instance normalization: The missing ingredient for fast stylization. *CoRR* abs/1607.08022.
- [Wang et al. 2016] Wang, G.; Lin, L.; Ding, S.; Li, Y.; and Wang, Q. 2016. Dari: Distance metric and representation integration for person verification. In *AAAI*.
- [Wang et al. 2018] Wang, J.; Zhu, X.; Gong, S.; and Li, W. 2018. Transferable joint attribute-identity deep learning for unsupervised person re-identification. In *CVPR*.
- [Wang et al. 2019] Wang, G.; Huang, P.; Xie, X.; and Lai, J. 2019. Spatial-temporal person re-identification.
- [Wang, Lai, and Xie 2017] Wang, G.; Lai, J.; and Xie, X. 2017. P2snet: Can an image match a video for person re-identification in an end-to-end way. *IEEE TCSVT* 99:1–1.
- [Wei et al. 2018] Wei, L.; Zhang, S.; Gao, W.; and Tian, Q. 2018. Person transfer gan to bridge domain gap for person re-identification. In *CVPR*.
- [Yu, Wu, and Zheng 2017] Yu, H.-X.; Wu, A.; and Zheng, W.-S. 2017. Cross-view asymmetric metric learning for unsupervised person re-identification. In *ICCV*.
- [Zhao et al. 2017a] Zhao, H.; Tian, M.; Sun, S.; Shao, J.; Yan, J.; Yi, S.; Wang, X.; and Tang, X. 2017a. Spindle net: Person re-identification with human body region guided feature decomposition and fusion. In *CVPR*, 1077–1085.
- [Zhao et al. 2017b] Zhao, L.; Li, X.; Zhuang, Y.; and Wang, J. 2017b. Deeply-learned part-aligned representations for person re-identification. In *ICCV*, 3219–3228.
- [Zheng et al. 2015] Zheng, L.; Shen, L.; Tian, L.; Wang, S.; Wang, J.; and Tian, Q. 2015. Scalable person re-identification: A benchmark. In *ICCV*, 1116–1124.
- [Zhong et al. 2018a] Zhong, Z.; Zheng, L.; Li, S.; and Yang, Y. 2018a. Generalizing a person retrieval model hetero- and homogeneously. In *ECCV*.
- [Zhong et al. 2018b] Zhong, Z.; Zheng, L.; Zheng, Z.; Li, S.; and Yang, Y. 2018b. Camera style adaptation for person re-identification. In *CVPR*.
- [Zhou et al. 2017] Zhou, J.; Yu, P.; Tang, W.; and Wu, Y. 2017. Efficient online local metric adaptation via negative samples for person re-identification. In *ICCV*.
- [Zhu et al. 2017] Zhu, J.-Y.; Park, T.; Isola, P.; and Efros, A. A. 2017. Unpaired image-to-image translation using cycle-consistent adversarial networks. In *ICCV*.
- [Zhuo et al. 2018] Zhuo, J.; Chen, Z.; Lai, J.; and Wang, G. 2018. Occluded person re-identification. *arXiv preprint arXiv:1804.02792*.